Membrane-Protein Interactions in a Generic Coarse-Grained Model for Lipid Bilayers

Beate West,[†*] Frank L. H. Brown,[‡] and Friederike Schmid[†]
[†]Fakultät für Physik, Universität Bielefeld, Bielefeld, Germany; and [‡]Department of Chemistry and Biochemistry and Department of Physics, University of California, Santa Barbara, California

ABSTRACT We study membrane-protein interactions and membrane-mediated protein-protein interactions by Monte Carlo simulations of a generic coarse-grained model for lipid bilayers with cylindrical hydrophobic inclusions. The strength of the hydrophobic force and the hydrophobic thickness of the proteins are systematically varied. The results are compared with analytical predictions of two popular analytical theories: The Landau-de Gennes theory and the elastic theory. The elastic theory provides an excellent description of the fluctuation spectra of pure membranes and successfully reproduces the deformation profiles of membranes around single proteins. However, its prediction for the potential of mean force between proteins is not compatible with the simulation data for large distances. The simulations show that the lipid-mediated interactions are governed by five competing factors: direct interactions; lipid-induced depletion interactions; lipid bridging; lipid packing; and a smooth long-range contribution. The mechanisms leading to hydrophobic mismatch interactions are critically analyzed.

INTRODUCTION

Membrane proteins are integral components of biomembranes and account for most of the biological processes that take place in and at membranes (1). Their activity often depends on their distribution within the membrane (2). The latter is determined by direct interactions, but also to a significant extent by indirect interactions, such as those mediated by the lipid bilayer matrix. Lipid-protein interactions are believed to play an important role, e.g., in controlling the aggregation and activity of gramicidin channels (3) and rhodopsin (4). Therefore, lipid-mediated interactions between membrane proteins or more generally membrane inclusions, have been studied intensely for many decades (5–7). Natural biomembranes are of course complex multicomponent systems, and membrane heterogeneities contribute critically to the lipid-protein interactions (8). However, a number of mechanisms have been identified that generate lipid-mediated protein interactions already in pure, one-component lipid bilayers.

1. The mechanism, which has been pointed out first in the literature, is the ''hydrophobic mismatch interaction'' (9–11). It arises in situations where the hydrophobic thickness of transmembrane proteins does not match the equilibrium bilayer thickness. The proteins then locally compress or expand the membrane, and the associated free energy penalty depends on their distribution in the membrane. This may induce protein clustering. The effect has been verified experimentally with systematic studies of gramicidin (12) and synthetic model peptides (13,14). Theoretically, it has been explained using different continuum theories for bilayers (15–32). However, it does not seem strong enough to fully account for the experimentally observed clustering of proteins in membranes (33,34).
2. Even in the absence of hydrophobic mismatch, inclusions locally disturb the translational and conformational degrees of freedom of lipids (9,35–41), which leads to local ''packing interactions'' (42). They have been analyzed theoretically by sophisticated mean-field studies of effective interactions between fully repulsive inclusions inserted in membranes of fixed thickness (37–39). These calculations generally predict attractive interactions at short distances and repulsive interactions at larger distances.
3. A third class of interactions discussed in the literature are ''fluctuation-induced interactions''. Proteins locally affect the elastic properties of the membranes—the bending rigidity and/or the spontaneous curvature—thereby changing the fluctuation spectrum of the membrane. The corresponding entropy change depends on the distribution of the proteins, which leads to Casimir forces (43–46).
4. In addition to these general interaction mechanisms, a number of more specific effects have been studied. For example, lipid-mediated interactions are observed between proteins that locally induce a strong membrane curvature. The sign of these interactions is not clear—whereas elastic theories predict repulsion, curvature-inducing proteins have in fact been found to aggregate in coarse-grained simulations (47). This indicates again that elastic theories alone cannot fully account for the effective interactions in such a system. Complex interaction mechanisms have also been predicted for membranes in low-temperature ordered, e.g., tilted states (48).

In this article, we study the interplay of different lipid-mediated interaction mechanisms between simple cylindrical inclusions in one-component lipid bilayers by computer simulations of a generic coarse-grained membrane model.

Submitted May 29, 2008, and accepted for publication September 4, 2008.

*Correspondence: west@physik.uni-bielefeld.de

Editor: Helmut Grubmuller.

0006-3495/09/01/0101/15 $2.00

doi: 10.1529/biophysj.108.138677

Despite being very simple, our model reproduces the main phases and conformationally driven phase transitions of pure lipid layers, including structures as complex as asymmetric and symmetric rippled states (49). It seems therefore suited to study generic phenomena that depend on lipid conformations. Specifically, we focus on the first two interaction mechanisms listed above, the hydrophobic mismatch interaction (mechanism 1), and the packing interactions (mechanism 2). The diameters of our inclusions are too small to generate measurable Casimir forces; they correspond roughly to those of simple β-helices. The inclusions do not induce curvature, and the bilayer is in the fluid state, hence additional interactions (mechanism 4) also do not contribute.

In the past decades, a number of computer simulation studies have focused on protein-lipid interactions, using both atomistic and coarse-grained models (see, e.g., (50,51) for recent overviews). Simulation studies of membrane-mediated protein-protein interactions are less abundant. Sintes and Baumgärtner (52) have been the first to study lipid-mediated interactions in a coarse-grained molecular model. They considered purely repulsive cylinders immersed in a bilayer of lipids which are head-grafted to opposing flat surfaces. In qualitative agreement with the mean-field theories cited above (37–39), they find an attractive depletion interaction at close distances followed by a repulsive well. Smeijers et al. (53) have studied the aggregation of proteins with different shapes in fusing vesicles. Very recently, de Meyer et al. (51) have presented a systematic study of lipid-mediated protein interactions for varying hydrophobic mismatch in a coarse-grained membrane model with soft dissipative particle dynamics interactions. Based on their data, they argue that an important factor driving the hydrophobic mismatch interaction is hydrophilic shielding, i.e., the influence of mismatch on the local arrangement of headgroups relative to tails.

This study is, in many respects, complementary to the work of de Meyer et al. (51).

First, our model is very different. Our coarse-grained lipid structure is much simpler than theirs; and we use hard-core, Lennard-Jones type interactions, similar to those used in atomistic or systematically coarse-grained models (54). This allows us to study the influence of local lipid packing phenomena, which are almost absent in systems with soft dissipative particle dynamics potentials, and to diagnose new factors that might contribute to the hydrophobic mismatch interaction, such as local chain ordering.

Second, we systematically vary the hydrophobicity of the protein and study its influence on the protein-protein interactions.

Third, we relate our simulation results to two popular analytical theories of lipid-induced interactions: The Landau-de Gennes theory (15–17) and the elastic theory for coupled monolayers (28–32). The elastic theory turns out to provide an excellent description of the peristaltic and bending fluctuations of pure membranes, and of thickness deformation profiles around single proteins. This allows us to analyze the elastic contribution to the protein-membrane interactions; among other things, we identify a mechanism by which they may be affected by hydrophilic shielding. The simulation results for the membrane-mediated protein-protein interactions, however, are not compatible with the predictions of the elastic theory, especially for large protein distances. In this case, the simpler Landau-de Gennes theory seems to perform better.

Our article is structured as follows: After introducing the model and the simulation method and briefly recollecting the main assumptions and predictions of the theories in the next section, we present and discuss our simulation results. We conclude with a brief summary.

MODELS AND METHODS

Simulation model and methods

We employ a simple generic lipid model (55) that has been shown to reproduce the characteristic high-temperature phase transitions of monolayers (56,57) and bilayers (49). The lipids are represented by chains of seven beads with one head bead of diameter σ_h followed by six tail beads of diameter σ_t. Beads, that are not direct neighbors in a chain interact, via a truncated and lifted Lennard-Jones potential,

$$V_{\text{bead}}(r) = \begin{cases} V_{\text{LJ}}(r/\sigma) - V_{\text{LJ}}(r_c/\sigma) & \text{if } r < r_c \\ 0 & \text{otherwise} \end{cases} \quad (1)$$

with

$$V_{\text{LJ}}(x) = \epsilon\left(x^{-12} - 2x^{-6}\right), \quad (2)$$

where σ is the mean diameter of the two interacting beads, $\sigma_{ij} = (\sigma_i + \sigma_j)/2$ ($i, j = h$ or t). Head-head and head-tail interactions are purely repulsive ($r_c = \sigma$) while tail-tail interactions also have an attractive contribution ($r_c = 2\sigma$). Within a lipid, chain beads are connected to each other by finitely extensible nonlinear elastic (FENE) springs with the spring potential

$$V_{\text{FENE}}(r) = -\frac{1}{2}\epsilon_{\text{FENE}}(\Delta r_{\max})^2 \log\left(1 - \left(\frac{r - r_0}{\Delta r_{\max}}\right)^2\right), \quad (3)$$

where r_0 is the equilibrium distance, $\Delta r_{\max}$ the maximal deviation, and ϵ_{FENE} the FENE spring constant. In addition, the chains are given bending stiffness by means of a bond-angle potential

$$V_{\text{BA}}(\theta) = \epsilon_{\text{BA}}(1 - \cos(\theta)). \quad (4)$$

The aqueous environment of the membrane is modeled with phantom solvent beads (58), which interact with lipids like head beads ($\sigma_s = \sigma_h$), but have no interactions with each other. Much like an implicit solvent, the phantom solvent is structureless and does not impart unwanted correlations onto the bilayers, and it is very cheap from a computational point of view. At sufficiently low temperatures, it forces the lipids to spontaneously self-assemble into stable bilayers (58).

Specifically our model parameters are (55,57) $\sigma_h = 1.1\sigma_t$, $r_0 = 0.7\sigma_t$, $\Delta r_{\max} = 0.2\sigma_t$, $\varepsilon_{\text{FENE}} = 100\ \varepsilon/\sigma_t^2$, and $\epsilon_{\text{BA}} = 4.7\epsilon$. The simulations were carried out at constant pressure $P = 2.\epsilon/\sigma_t^3$ and temperature $k_BT = 1.3\epsilon$, which is well in the fluid phase region of the bilayer. (The bilayer undergoes a main transition to a tilted gel phase $L_{\beta'}$ via a ripple phase $P_{\beta'}$ at the temperature $k_BT = 1.2\epsilon$ (49).) Comparing the monolayer thickness, $t_0 \sim 3\sigma_t$, and the area per lipid, $a_0 \sim 1.36\sigma_t^2$, with the corresponding numbers for real lipid bilayers in the fluid L_α phase, we find that the values in our model roughly reproduce those of dipalmitoyl phosphatidylcholine (DPPC) bilayers, if we set $\sigma_t \sim 6$ Å (59). By matching the temperatures of the main transition ($T_m = 42°$C in DPPC) we can also identify an energy scale: $\epsilon \sim 0.36 \times 10^{-20}$ J.

The proteins are modeled as cylinders with the radius $R = 1.5\sigma_t$, which have fixed orientation along the bilayer normal (the z axis). We impose the orientation to realize the situation considered in the elastic theory as closely as possible—proteins cannot respond to hydrophobic mismatch by tilting. In a real membrane, this would correspond to a situation where the orientation of the transmembrane domain of a protein is kept fixed by external factors, e.g., geometrical constraints in the extramembrane domain. For comparison, selected simulations were also conducted for proteins that were allowed to tilt (unconstrained orientations). As in other model studies (31,51), the effect of orientation fluctuations on the results was found to be rather small (see Simulation Results).

The interaction between proteins and lipid or solvent beads has a purely repulsive contribution, which is described by a radially shifted and truncated Lennard-Jones potential

$$V_{\mathrm{rep}}(r) = \begin{cases} V_{\mathrm{LJ}}((r-\sigma_0)/\sigma) - V_{\mathrm{LJ}}(1) & \text{if } r-\sigma_0 < \sigma \\ 0 & \text{otherwise} \end{cases}, \tag{5}$$

where $r = \sqrt{x^2+y^2}$ denotes the distance of the interacting partners in the xy plane, the parameter σ is given by $\sigma = (\sigma_t + \sigma_i)/2$ for interactions with beads of type i ($i = h$, t, and s for head, tail, and solvent beads, respectively), $\sigma_0 = \sigma_t$, and V_{LJ} has been defined above (Eq. 2). The direct protein-protein interactions have the same potential (Eq. 5) with $\sigma = \sigma_t$ and $\sigma_0 = 2\sigma_t$.

In addition, protein cylinders attract tail beads on a hydrophobic section of length L. This is described by an additional attractive potential that depends on the z distance between the tail bead and the protein center. The total potential reads

$$V_{\mathrm{pt}}(r,z) = \varepsilon_{\mathrm{pt}}\big(V_{\mathrm{rep}}(r) + V_{\mathrm{attr}}(r) \times W_{\mathrm{P}}(z)\big), \tag{6}$$

with the attractive Lennard-Jones contribution

$$V_{\mathrm{attr}}(r) = \begin{cases} V_{\mathrm{LJ}}(1) - V_{\mathrm{LJ}}(2) & \text{if } r-\sigma_0 < \sigma \\ V_{\mathrm{LJ}}((r-\sigma_0)/\sigma) - V_{\mathrm{LJ}}(2) & \text{if } \sigma < r-\sigma_0 < 2\sigma \\ 0 & \text{otherwise} \end{cases} \tag{7}$$

and a weight function $W_{\mathrm{P}}(z)$, which is unity on a stretch of length $L - 2\sigma_t$ and crosses smoothly over to zero over a distance σ_t at both sides. Specifically, we use

$$W_{\mathrm{P}}(z) = \begin{cases} 1 & \text{if } |z| \le l \\ \cos^2[3/2(|z|-l)] & \text{if } l < |z| < l + \pi/3 \\ 0 & \text{otherwise} \end{cases} \tag{8}$$

with $l = L/2 - \sigma_t$. The parameter ϵ_{pt} tunes the strength of the lipid-protein interaction, i.e., the hydrophobicity of the protein. It was varied between $\epsilon_{\mathrm{pt}} = 1$ and $\epsilon_{\mathrm{pt}} = 6$. The hydrophobicity $\epsilon_{\mathrm{pt}} = 1$ was sufficient to trap the center of the protein inside the membrane: The fluctuations of its z position relative to the height of the membrane h were $\langle (z_{\mathrm{protein}} - h)^2 \rangle \le 0.5\sigma_t$ for all values of ϵ_{pt}. The proteins with unconstrained orientation were modeled as spherocylinders of length L with essentially the same interaction potentials, except that the z axis is replaced by the protein axis, and the variable r by the closest distance to the protein.

The system is studied using Monte Carlo simulations at constant pressure and temperature with periodic boundary conditions in a simulation box of variable size and shape: The simulation box is a parallelepiped spanned by the vectors $(L_x, 0, 0)$, $(s_{yx}L_x, L_y, 0)$, $(s_{zx}L_x, s_{zy}L_y, L_z)$, and all L_i and s_j are allowed to fluctuate. This ensures that the membranes have no interfacial tension. The system sizes ranged from 200 to 3200 lipids, and the simulations were run up to 8,000,000 Monte Carlo steps, where one Monte Carlo step corresponds to one Monte Carlo move per bead. Moves that alter the simulation box were attempted every 50th Monte Carlo step. To generate the initial configurations, we set up a perfectly ordered bilayer in the xy plane with straight chains pointing in the z direction and simulated it until it was equilibrated, i.e., all observables of the system fluctuated about the equilibrium value and none of the observables shows a trend. Typical equilibration times were 1,000,000 Monte Carlo steps (4,000,000 Monte Carlo steps in simulations where we looked at large-scale height fluctuations). Due to this procedure, the bilayers were oriented in the xy plane.

Fig. 1 shows two snapshots of a system containing two inclusions whose thickness roughly matches that of the bilayer ($L = 6\sigma_t$), with different hydrophobicity parameters ϵ_{pt}. They illustrate the existence of membrane-mediated attractive interactions even in the absence of hydrophobic mismatch. At low values of ϵ_{pt}, the proteins touch. At higher values of ϵ_{pt}, they are separated by a single lipid layer.

Before proceeding to a more quantitative discussion of the simulation results, we shall now briefly recollect the main assumptions and results of the analytical theories that we use to analyze our data.

Landau-de Gennes theory

One of the oldest theoretical approaches to studying lipid-mediated interactions between inclusions is based on a Landau-de Gennes expansion of the free energy in powers of the lipid area or membrane thickness variations (15–17,60). In the simplest case, this expansion reads (17)

$$F_{\mathrm{LdG}} = \int \mathrm{d}^2 r \left\{ \frac{a}{2}(2\phi_{\mathrm{LdG}})^2 + \frac{c}{2}(2\nabla\phi_{\mathrm{LdG}})^2 \right\} \tag{9}$$

with the boundary condition $\phi_{\mathrm{LdG}} = t_R$ at the surface of the inclusion, where ϕ_{LdG} denotes the local deviation of the monolayer thickness from its equilibrium value t_0 in the unperturbed membrane, and $2(t_R + t_0)$ is the hydrophobic thickness of the inclusion. The first term in Eq. 9 accounts for the area compressibility k_A of the bilayer ($k_A = a(2t_0)^2$), and the second term penalizes spatial thickness variations, i.e., the variable c is taken to be positive. Minimizing this free energy for a membrane containing a single inclusion at $r = 0$ yields the deformation profile

$$\phi_{\mathrm{LdG}}(r) = t_{\mathrm{R}} \frac{K_0(r/\xi)}{K_0(R/\xi)}, \tag{10}$$

where R is the radius of the inclusion, $\xi = \sqrt{c/a}$ the correlation length, and K_0 is the modified Bessel function of the second kind. For $r\xi > 1$, Eq. 10 can be approximated by an exponential decay

$$\phi_{\mathrm{LdG}}(r) \approx t_{\mathrm{R}} \exp\left(-\frac{r-R}{\xi}\right)\sqrt{\frac{R}{r}}. \tag{11}$$

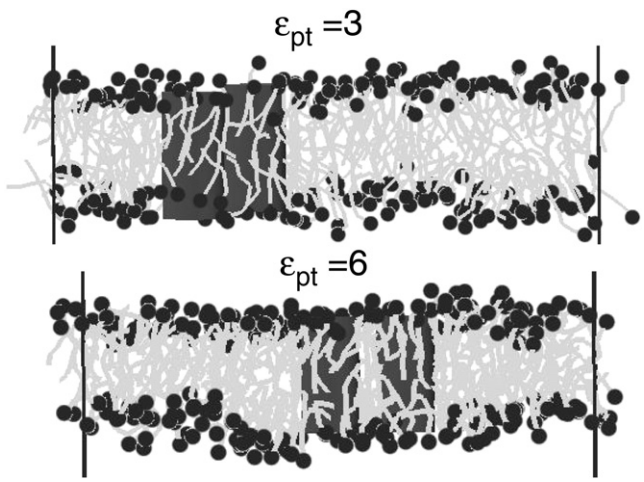

FIGURE 1 Cross-section snapshot of a model membrane with two inclusions of hydrophobic thickness $L = 6\theta_{\mathrm{t}}$ and different hydrophobicity parameter $\epsilon_{\mathrm{pt}} = 3$ (*top*) and $\epsilon_{\mathrm{pt}} = 6$ (*bottom*). Light shaded lines show tail bonds, dark circles the heads (not to scale), dark cylinders the inclusions.

Such exponential laws have often been used to fit data from simulations or molecular theories for membranes with inclusions (19,20,60–62). Equation 9 can also be used to deduce an equation for the monolayer thickness fluctuation spectrum

$$\left\langle \left|\phi_{\mathrm{LdG}}(q)\right|^2 \right\rangle = \frac{k_{\mathrm{B}}T}{4(a + cq^2)}. \tag{12}$$

Elastic theory

Another popular approach is the elastic theory of coupled monolayers (23–32,63). Here the membrane is treated as a system of two coupled elastic monolayer sheets. The basic structure of the different theories is very similar—they differ mainly in the choice of the boundary conditions and the number of elastic terms that they include. For example, early theories have often disregarded the possibility that the individual monolayers may have a spontaneous curvature, whereas this is usually accounted for in more recent work. Here we shall use a recent version of the elastic theory developed by Brannigan and Brown (31,32), which is fairly complete in the sense that it includes all known elastic terms.

We consider a flat lipid bilayer in the xy plane. The two constituting monolayers are described by four independent fluctuating fields—two accounting for mesoscopic bending deformations, and two for the microscopic protrusions. We assume that the volume of lipids is locally conserved, and that the mesoscopic bilayer height and thickness fluctuations and the protrusions basically decouple. The latter requirement may seem all-too rigid and is actually not imposed in the original model (31), but it leads to a considerable simplification of the resulting theory and will be justified a posteriori by the fact that it describes the fluctuation spectra of our model bilayers in an excellent way.

The quantities of interest for us are the local bilayer height h, the local monolayer thickness t, and the local field ϕ_{el}, which denotes just the contribution of bending deformations to the thickness, without the microscopic protrusions. This field is defined in analogy to the field ϕ_{LdG} in Eq. 9. With the assumptions mentioned above, the spectra of the bilayer height and monolayer thickness fluctuations in Fourier space, $\langle|h(q)|^2\rangle$ and $\langle|t(q)|^2\rangle$, are given by (31)

$$\left\langle \left|h(q)\right|^2 \right\rangle = \frac{k_{\mathrm{B}}T}{k_c q^4} + \frac{k_{\mathrm{B}}T}{2(k_\lambda + \gamma_\lambda q^2)}, \tag{13}$$

$$\left\langle \left|t(q)\right|^2 \right\rangle = \frac{k_{\mathrm{B}}T}{k_c q^4 - 4k_c\zeta q^2/t_0 + k_A/t_0^2} + \frac{k_{\mathrm{B}}T}{2(k_\lambda + \gamma_\lambda q^2)}, \tag{14}$$

where k_c and k_A are the bending and the compressibility moduli of the bilayer; ζ is related to the spontaneous curvature (the parameter ζ is given by $\zeta = c_0 - \mathrm{d}c_0/\mathrm{d}\Sigma\times\Sigma$, where Σ is the area per lipid, evaluated for flat equilibrium membranes without inclusions); t_0 is the mean monolayer thickness; and the parameters γ_λ and k_λ characterize the protrusions. Fitting our simulation data to these theoretical spectra allows us to 1), test the validity of the theory; and 2), extract the elastic parameters k_c, k_A, and ζ, which we need for the subsequent analysis of protein-lipid interactions.

Within the decoupling approximation, the protrusions and the height fluctuations do not contribute to the protein-induced membrane deformations. The free energy of monolayer thickness deformations can be expressed as (32)

$$F_{\mathrm{el},0} = \int d^2r \Big\{ \frac{k_A}{2t_0^2}\phi_{\mathrm{el}}^2 + 2k_c c_0 \nabla^2\phi_{\mathrm{el}} + 2k_c\zeta\frac{\phi_{el}}{t_0}\nabla^2\phi_{\mathrm{el}} + \tfrac{k_c}{2}\left(\nabla^2\phi_{\mathrm{el}}\right)^2 + k_G \det\left(\partial_{ij}\phi_{\mathrm{el}}\right) \Big\}, \tag{15}$$

where $(\phi_{\mathrm{el}} + t_0)$ is the locally smoothed monolayer thickness (without the protrusions), and we have introduced the spontaneous curvature of the monolayers c_0 and the Gaussian rigidity k_G. According to the Gauss-Bonnet theorem, the latter only contributes an uninteresting constant in homogeneous planar sheets and is thus often omitted; in the presence of inclusions (holes), however, it has to be taken into account (32).

We consider inclusions with radius R that enforce a certain membrane thickness $2t_R$ at their surface. To calculate the deformation profile of the bilayer in the vicinity of such an inclusion centered at $r = 0$, we minimize the free energy $F_{\mathrm{el},0}$ with respect to the profile $\phi_{\mathrm{el}}(r)$ while keeping the membrane deformation at the surface of the inclusion fixed, $\phi_{\mathrm{el}}^{\mathrm{surface}} \equiv t_R$. This leads to the Euler-Lagrange equation

$$\frac{k_A}{k_c t_0^2}\phi_{\mathrm{el}} + \frac{4\zeta}{t_0}\nabla^2\phi_{\mathrm{el}} + \nabla^4\phi_{\mathrm{el}} = 0, \tag{16}$$

with the boundary conditions

$$\phi_{\mathrm{el}}(R) = t_R \tag{17}$$

$$\nabla_r^2\phi_{\mathrm{el}}|_R = -\frac{k_G}{k_c R}t'_R - 2\left(c_0 + \zeta\frac{t_R}{t_0}\right) \tag{18}$$

at the surface of the inclusion, and

$$\partial_r\phi_{\mathrm{el}}(r)|_{r\to\infty} = \nabla_r^3\phi_{\mathrm{el}}(r)|_{r\to\infty} = 0 \tag{19}$$

at infinity, where $\nabla^2{}_r = (1/r)\partial_r r\partial_r$ and $\nabla^3{}_r = \partial_r\nabla^2{}_r$, and we have defined $t'_R = \partial_r\phi_{\mathrm{el}}|_R$. For a single inclusion, these equations can be solved analytically, giving (30)

$$\phi_{\mathrm{el}}(r) = A_1 J_0(\alpha_+ r) + A_2 Y_0(\alpha_+ r) + A_3 J_0(\alpha_- r) + A_4 Y_0(\alpha_- r) \tag{20}$$

with

$$\alpha_\pm = \sqrt{\frac{2\zeta}{t_0} \pm \sqrt{\left(\frac{2\zeta}{t_0}\right)^2 - \frac{k_A}{k_c t_0^2}}}, \tag{21}$$

where $J_0(x)$ and $Y_0(x)$ are the 0^{th}-order Bessel functions of the first and second kind, and the coefficients A_i are determined by the boundary conditions. (We note that this expression differs from those given in (30) and (32), which also are mutually different. In both articles, the corresponding equations contain typographical errors.)

The elastic model presented so far only uses material properties of free, bulk membranes. Inclusions may locally alter the lipid properties, e.g., the lipid volume, the lipid ordering etc., which may in turn affect the elastic properties (e.g., the equilibrium thickness, the spontaneous curvature, the bending rigidity, the compression modulus) of the membrane. Brannigan and Brown (32) have demonstrated for the case of varying lipid volume that such effects can be incorporated into the theory in a relatively straightforward way.

Here we will discuss this from a more general perspective: Consider some scalar quantity $q(r)$ that is distorted from its bulk value q_0 by the inclusion and locally alters the membrane properties. By symmetry, it will introduce two new terms in Eq. 15,

$$F_{\mathrm{el},q} = F_{\mathrm{el},0} + F_q \quad \text{with} \quad F_q = \int \mathrm{d}^2r \left\{ K_1\frac{\delta q}{q_0}\phi_{\mathrm{el}} + K_2\frac{\delta q}{q_0}\nabla^2\phi_{\mathrm{el}} \right\}. \tag{22}$$

Here $\delta q/q_0$ denotes the relative deviation of q, and terms that do not depend on ϕ_{el} or that are of higher than quadratic order in the deviations ϕ_{el} and $\delta q/q_0$ have been disregarded. In general, the additional free energy contribution F_q will change the Euler-Lagrange equations, and the solution Eq. 20 is no longer valid close to the inclusion. The situation, however, simplifies considerably if we make the reasonable assumption that the local

distortion $\delta q(r)$ decays to zero on a length scale that is much smaller than the characteristic length scales of the elastic profile. For an inclusion centered at $r = 0$, we can then replace $\phi_{\rm el}(r)$ by $t_R + t'_R(r - R)$ in Eq. 22, and the free energy F_q turns into a surface term,

$$F_q = t_R K_1 \int_R^\infty 2\pi dr\, r\frac{\delta q(r)}{q_0} + t'_R \int_R^\infty dr 2\pi \frac{\delta q(r)}{q_0}(K_1\ r(r-R) + K_2), \quad (23)$$

which only changes the boundary condition Eq. 18: The local distortion $\delta q(r)$ renormalizes the spontaneous curvature term in Eq. 18 according to

$$\tilde{c}_0 = c_0 - \frac{1}{2k_c R}\int_R^\infty dr \frac{\delta q(r)}{q_0}(K_1 r(r-R) + K_2). \quad (24)$$

Inserting that into Eq. 22 with Eq. 15 and exploiting the Euler Lagrange equation (Eq. 16), we find that the free energy of the deformation is given by

$$F_{{\rm el},q} = \pi k_c R\left(t_R \nabla_r^3 \phi_{\rm el}|_R - 2t'_R\left(\tilde{c}_0 - \zeta t_R/t_0\right)\right) + \text{constant}, \quad (25)$$

where the constant does not depend on the deformation profile.

This result can readily be generalized to situations where several scalar quantities $q_\alpha(r)$ affect the membrane simultaneously. Within our linear approximation, each of them will contribute a separate surface term F_{q_α} of the form from Eq. 23 and the effect on the renormalized curvature term in Eq. 24 will be additive. For given renormalized curvature $\tilde{c}_0$, Eq. 25 still remains valid.

Our findings agree qualitatively with those of Brannigan and Brown (32), who also conclude that lipid volume deviations $v(r)/v_0$ at the surface of the inclusion effectively renormalize the spontaneous curvature term. The actual expression for $\tilde{c}_0$ given in that article is different from ours. The discrepancy is due to an error in the original analysis.

Other theories

The elastic theory sketched in the previous section is an effective interface theory, i.e., the main degrees of freedom are the positions of the fluctuating interfaces between the monolayers and the surrounding solvent. A number of authors have put forward elastic theories that include the local tilt of chains as supplementary degrees of freedom in the spirit of the Landau-de Gennes theory for smectic liquid crystals (22,48,66,67). These theories introduce new elastic parameters that describe, e.g., the splay, twist, and bend modes of the tilt order parameter, and their coupling to the interfacial degrees of freedom. Due to the difficulty of accessing the additional parameters, they are not included in this analysis.

Another entirely different type of approach is pursued by the molecular theories (19,20,36–39,68). They account for the chain character of lipids explicitly and calculate the packing interactions between proteins and membranes by different sophisticated mean-field methods. Since the results depend on the chain model, which is different from ours, they can only be compared to our simulation data at a qualitative level (see next section).

SIMULATION RESULTS

We turn to discuss the simulation results. First, we consider the properties of pure bilayers, with no inclusions. The results confirm the validity of the elastic theory for our system, and provide values for the elastic parameters that can be used subsequently. Second, we investigate the deformation profiles of a membrane in the vicinity of single inclusions. Third, we study the effective inclusion-inclusion interactions for inclusions with different hydrophobic lengths and hydrophobicity parameters.

Elastic properties of the pure membrane

One of the most powerful approaches to looking at elastic membrane properties is the analysis of fluctuation spectra (69–72). To determine the spectra for our membranes, we have basically followed the procedure outlined in Loison et al. (72). We have carried out simulations of a bilayer containing 3200 lipids (and 24,615 solvent beads). The system was divided in $N_x \times N_y$ bins in the xy plane with $N_x = N_y = 20$. In each bin, the z value of the mean head position in the z direction was determined for both monolayers separately. The average and the difference of the two values give the bilayer height spectrum $h(x, y)$ and monolayer thickness spectrum $t(x, y)$, respectively. The two spectra were then Fourier-transformed according to

$$f_{q_x,q_y} = \frac{L_x L_y}{N_x N_y}\sum_{x,y} f(x,y)e^{-i(q_x x + q_y y)} \quad (26)$$

and the values of $|h_q|^2$ and $|t_q|^2$ were collected in q bins of size 0.1. The binning was made necessary by the fact that the dimensions of the simulation box and hence the q values fluctuate. In each bin, the averages $\langle|h_q|^2\rangle$ and $\langle|t_q|^2\rangle$ were evaluated.

The results are shown in Fig. 2. The data illustrates the characteristic features of the spectra: The height fluctuations

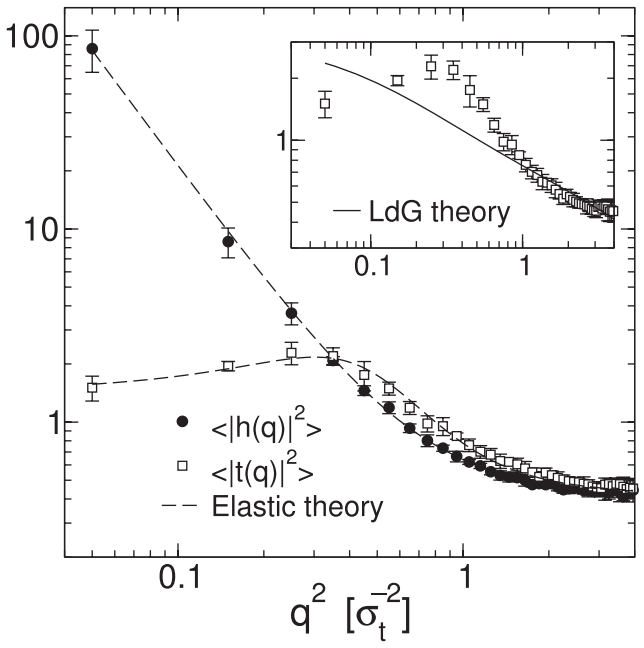

FIGURE 2 Fourier spectra of height (*solid circles*) and thickness fluctuations (*open squares*). The dashed line shows a fit of the data to the elastic theory (31) (Eqs. 13 and 14). The inset shows the thickness data alone with a fit to the Landau-de Gennes theory (Eq. 12).

TABLE 1 Elastic constants of our model membrane as obtained from a fit of the fluctuation spectra of pure membranes to the elastic theory

Parameter	Value (LJ units)	Value (SI units)
k_c	$6.2 \pm 0.4\ \epsilon$	2.2×10^{-20} J
ζ/t_0	$0.15 \pm 0.09\ \sigma_t^{-2}$	0.42 nm^{-2}
$k_A/{t_0}^2$	$1.3 \pm 0.3\ \epsilon\sigma_t^{4}$	3.6×10^{-20} J/nm^4
c_0	$-0.05 \pm 0.02\ \sigma_t^{-1}$	-0.08 nm^{-1}
k_G	-0.26 [-2.8–0] ϵ	$-1 - 0 \times 10^{-20}$ J
k_λ	$1.5 \pm 1\ \epsilon/\sigma_t^{4}$	4.2×10^{-20} J/nm^4
γ_λ	$0.007 \pm 0.01\ \epsilon/\sigma_t^{2}$	0.7×10^{-22} J/nm^2

Values in SI units are estimates based on the identification $\sigma_t \sim 6$ Å and $\epsilon \sim 0.36 \times 10^{-20}$ J (see text for explanation).

are Goldstone modes, hence the height spectrum diverges for small wavelength modes. In contrast, the monolayer thickness spectrum is limited by the equilibrium thickness and tends toward a constant value for small wavevector values (70). It exhibits a characteristic peak at $q^2{\sigma_t}^2 \sim 0.4$, corresponding to a soft peristaltic mode with wavelength $\sim 10\sigma_t$. At small q^2, the fluctuation spectra are dominated by bending deformations. For larger values of q^2, the spectra are dominated by the protrusion modes and are equal for the height and the monolayer thickness fluctuations.

The solid line in Fig. 2 (main frame) shows the fit to the elastic theory, Eqs. 13 and 14, with fit parameters k_c, ζ/t_0, ${k_A}/{t_0}^2$, k_λ, and γ_λ. The results of the fit are given in Table 1. The elastic theory describes the data in an excellent way. This confirms the validity of the underlying assumptions, most notably, the decoupling approximations (see above). The strength of the coupling between bending modes and protrusion modes can be estimated by looking at the coupling parameter ${\gamma_\lambda}^2/k_\lambda k_c$. Our fit gives ${\gamma_\lambda}^2/k_\lambda \mathrm{k}_c = 5 \times 10^{-6}$, which is indeed much smaller than unity. The inset of Fig. 2 shows the fit of the monolayer thickness spectrum to the Landau-de Gennes theory (*solid line*). To make the analyses comparable, we have included a protrusion contribution and fitted the monolayer thickness deformations to

$$\left\langle |t(q)|^2 \right\rangle = \frac{k_\mathrm{B}T}{4(a + cq^2)} + \frac{k_\mathrm{B}T}{2(k_\lambda + \gamma_\lambda q^2)} \qquad (27)$$

(compare to Eq. (12)) and the bending deformations to Eq. 13 simultaneously, with fit parameters a, c, k_c, k_λ, and γ_λ. Not surprisingly, the Landau-de Gennes theory cannot reproduce the peak at nonzero q in $\langle |t(q)|^2 \rangle$, hence it misses one important characteristic of the thickness spectrum.

Turning back to the elastic theory, the analysis of fluctuation spectra yields the values of three elastic parameters that are needed in the subsequent analysis: the bending rigidity k_c, the compressibility modulus k_A, and the extrapolated curvature ζ. The two remaining elastic parameters in Eq. 15 are the spontaneous curvature c_0, and the Gaussian rigidity k_G. Under the (admittedly bold) assumption that the two monolayer slabs can be treated as elastic continua subject to internal stress, these quantities can be calculated from the first and the second moment of the surface tension profile across the monolayers (73) via

$$k_c\, c_0 = -\int_0^\infty \mathrm{d}z\, \gamma_\mathrm{int}(z)(z - z_0), \qquad (28)$$

$$k_G = 2\int_0^\infty \mathrm{d}z\, \gamma_\mathrm{int}(z)(z - z_0)^2. \qquad (29)$$

Here $\gamma_\mathrm{int}(z)$ denotes the intrinsic surface tension profile, which is defined as the difference between the normal and the tangential components of the local pressure tensor. The integration starts at the bilayer midplane $z = 0$, and the reference plane $z = z_0$ is the inextensibility plane, i.e., the plane in which an infinitesimal volume element is not compressed or extended if the monolayer is bent. For symmetric bilayers with overall tensionless monolayers, one has $\int_0^\infty \mathrm{d}z\, \gamma_\mathrm{int}(z) = 0$, and the result for c_0 is independent of z_0. The value obtained for k_G, however, depends sensitively on the choice of z_0.

In the simulation, the pressure tensor is obtained using the virial theorem,

$$\mathrm{P}_{\alpha\beta} = \frac{Nk_\mathrm{B}T}{V}\delta_{\alpha\beta} + \frac{1}{2V}\left\langle \sum_i r_i^\alpha F_i^\beta \right\rangle, \qquad (30)$$

where $\mathbf{r}_i$ is the position of particle i, $\mathbf{F}_i$ the force acting on this particle, N the number of particles, T the temperature, and V the volume. Because of the periodic boundaries, care must be taken to use a version of the expression (Eq. 30) that does not depend on absolute positions, e.g., by rewriting the contribution of pairwise forces as $\sum_{i<j}(r_i^\alpha - r_j^\alpha)F_{ij}^\alpha$, etc. The pressure tensor of the whole equilibrated system is diagonal, $\mathrm{P}_{\alpha\beta} = \delta_{\alpha\beta}P$, where P is the applied pressure. Nevertheless, it varies spatially on the molecular scale. To measure the local pressure profile, we divide the system along the z axis in slices of length $\delta z = 0.125\sigma$. The contributions of pairwise forces to the total virial are parceled out on the bins according to the Irving-Kirkwood convention (74), i.e., they are distributed evenly on the line connecting the two interaction partners. The contributions of our only multibody interactions, the bond-angle potentials (Eq. 4), are distributed evenly on the two participating bonds. Alternatively, Goetz and Lipowsky (75) have proposed a method where the contribution of multibody forces is spread evenly on all lines connecting the participating partners (the bond-angle virials would then be distributed on triangles). We have also implemented this definition, and found that the effect on the pressure profile was negligible. The interfacial tension profile is given by

$$\gamma(z) = \mathrm{P}_{zz}(z) - \frac{1}{2}\big(\mathrm{P}_{xx}(z) + \mathrm{P}_{yy}(z)\big). \qquad (31)$$

Fig. 3 shows the surface tension profiles of a pure model membrane for four system sizes. Qualitatively, it exhibits

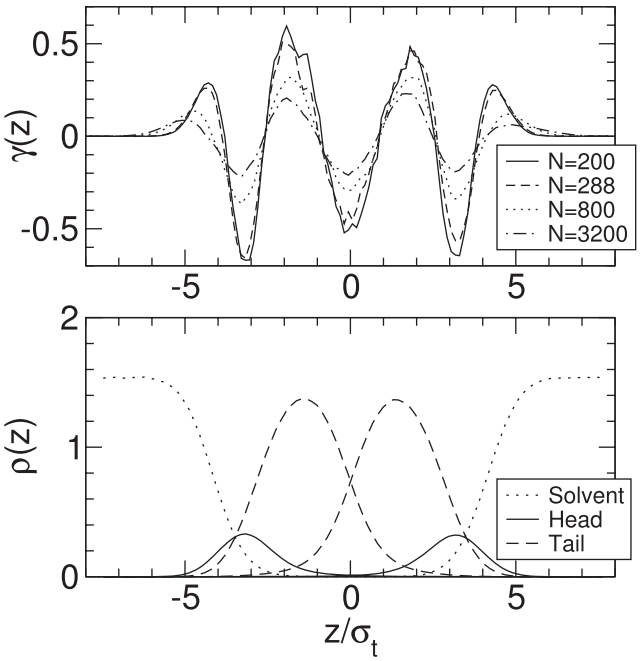

FIGURE 3 Surface tension profile $\gamma(z)$ for four different system sizes with $N = 200$, 288, 800, and 3200 lipids (*top panel*). The bottom panel shows the corresponding density profiles of solvent, head and tail beads in the smallest system (200 lipids) for comparison.

the same features as the stress profile obtained with the similarly simple coarse-grained lipid model of Goetz and Lipowsky (75). Most notably, the surface tension features a negative peak in the bilayer midplane (at $z = 0$), indicating that the monolayers are strongly bound to each other, in agreement with atomistic and coarse-grained simulations of DPPC bilayers (54,62,76) (S.-J. Marrink, 2008, personal communication).

Due to the height fluctuations, $\gamma(z)$ depends on the lateral system size: All profiles are broadened in large systems. In contrast, Eqs. 28 and 29 are based on a hypothetical intrinsic surface tension profile $\gamma_{\rm int}(z)$. If such an intrinsic profile exists, the actual tension profile $\gamma(z)$ should be given by the convolution of $\gamma_{\rm int}(z)$ with the distribution of interface heights $W(z')$,

$$\gamma(z) = \int \mathrm{d}z'\, W(z')\, \gamma_{\rm int}(z - z'). \qquad (32)$$

In this case, one easily verifies that the integral $\Gamma_0 = \int \mathrm{d}z\ \gamma(z)$ is still zero for tensionless membranes, and the second moment $\Gamma_2 = \int \mathrm{d}z\ z^2\ \gamma(z)$ does not depend on the shape of the function $W(z)$ for symmetric tensionless bilayers with $\int \mathrm{d}z\ z\ \gamma(z) = 0$. This prediction can be used to test the convolution hypothesis in Eq. 32. The integral Γ_0 is close to zero in all systems as expected ($\Gamma_0\ \sigma_t^2/\epsilon = -0.018$, -0.003, -0.04, and 0.02 for the system with $N =$ 200, 288, 800, and 3200 lipids, respectively). The values of the second moment are $\Gamma_2/\epsilon = 2.8$, 2.7, 2.0, and 2.8. Hence Γ_2 does not depend on the system size, which confirms the existence of an intrinsic tension profile.

We note that the integral for the Gaussian rigidity (Eq. 29) still depends on the system size, since the lower integration bound is finite. Both Eqs. 28 and 29 are only applicable in sufficiently small systems. Therefore, we proceed by evaluating them in the smallest system with $N = 200$ lipids. For the monolayer curvature, we obtain a small negative value, $k_c c_0 = -0.3 \pm 0.1\epsilon/\sigma_t$. This may seem surprising, given the fact that the heads in our model are larger than the tail beads, and that the tails have to tilt in the low temperature phase (the $L_{\beta'}$ phase) to accommodate this mismatch. Indeed, the spontaneous curvature is found to be positive in the gel state (B. West, unpublished data). At higher temperature, the tails disorder and occupy more membrane area, and c_0 decreases and changes sign as a result. Negative curvatures have also been found in more realistic models of DPPC bilayers (54). The calculated result for the Gaussian rigidity depends on the position of the inextensibility plane z_0, which is not known unambiguously. Depending on our choice of z_0, we obtain k_G values that range between $\pm 2.8\epsilon$. Among these, the positive values can be excluded: Positive Gaussian rigidity would imply that the bilayers tend to assume saddle-shaped configurations, which destabilizes flat bilayer structures on large scales and promotes interconnected structures, i.e., cubic phases or spongelike structures. Our model bilayers remained flat for all system sizes. Therefore, only negative values of k_G are physically reasonable. In previous work (32), z_0 was taken to be the neutral plane where $\gamma(z)$ crosses zero, i.e., $z_0 = 2.6\sigma_t$ in our system (compare to Fig. 3). Using this value, we obtain $k_G = -0.26\epsilon$.

To summarize this subsection, the Landau-de Gennes theory does not describe the fluctuations of our model membranes very well. It misses a soft peristaltic mode in the monolayer thickness spectrum, which is clearly present in the simulation data. In contrast, the elastic theory fits the data excellently. We have extracted values for the elastic parameters that describe the bending deformations in monolayers from the fluctuation spectra and the surface tension profiles of bilayers. They are given in Table 1. Using the identifications $\sigma_t \sim 6$ Å and $\epsilon \sim 0.36 \times 10^{-20}$J (see Models and Methods), we can relate our model to real lipid bilayers. The values of our elastic parameters in SI units (see Table 1) have the same order of magnitude as those obtained based on all-atom simulations of DPPC (70), $k_c \sim 4 \times 10^{-20}$ J, $k_A/{t_0}^2 \sim 1.1 \times 10^{-20}$ J/nm^4, $\zeta/t_0 \sim 0.18$ nm^{-2} (31), and $c_0 \sim -0.04$ to -0.05 nm^{-1} (54), and those based on experimental estimates (79), $k_c \sim 5 - 20 \times 10^{-20}$ J, $k_A/{t_0}^2 \sim 6 \times 10^{-20}$ J/nm^4, $c_0 \sim -0.04$ nm^{-1}, and $k_G/k_c \sim -0.8$.

Deformation of a bilayer by a single protein

Next we investigate the deformation of a bilayer by a single inclusion. To this end, we consider the radial profiles of the membrane thickness 2ϕ, which we define as the mean z distance between the head positions in the upper and the lower

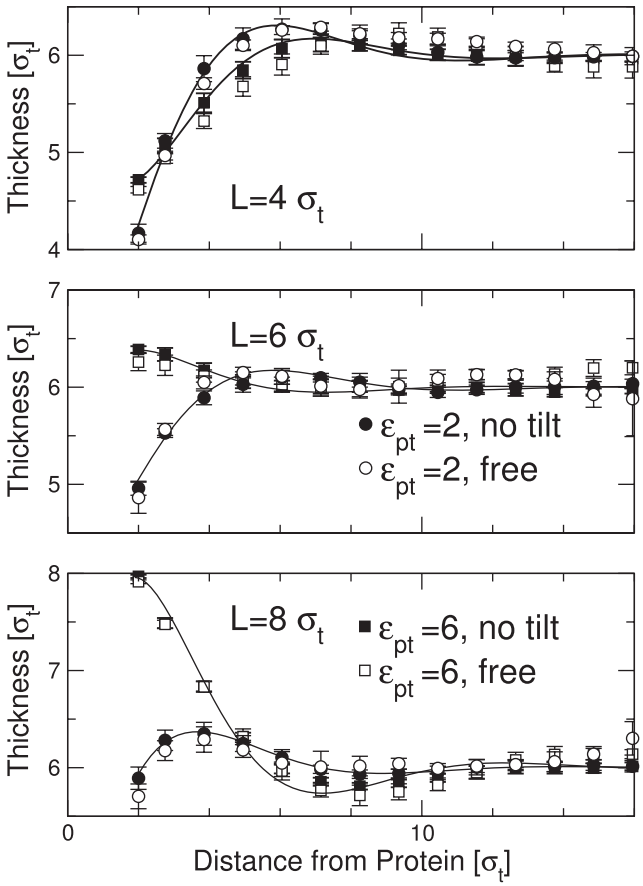

FIGURE 4 Radial membrane thickness profiles in the vicinity of inclusions with different hydrophobic thickness L and hydrophobicity parameter ϵ_{pt} as indicated. Solid symbols show data for inclusions with fixed orientation along the z axis, open symbols correspond to unconstrained inclusions. The solid and dashed lines are fits to the elastic theory (Eqs. 20 with 17 and 18) with fit parameters t_R and $\tilde{c}_0$.

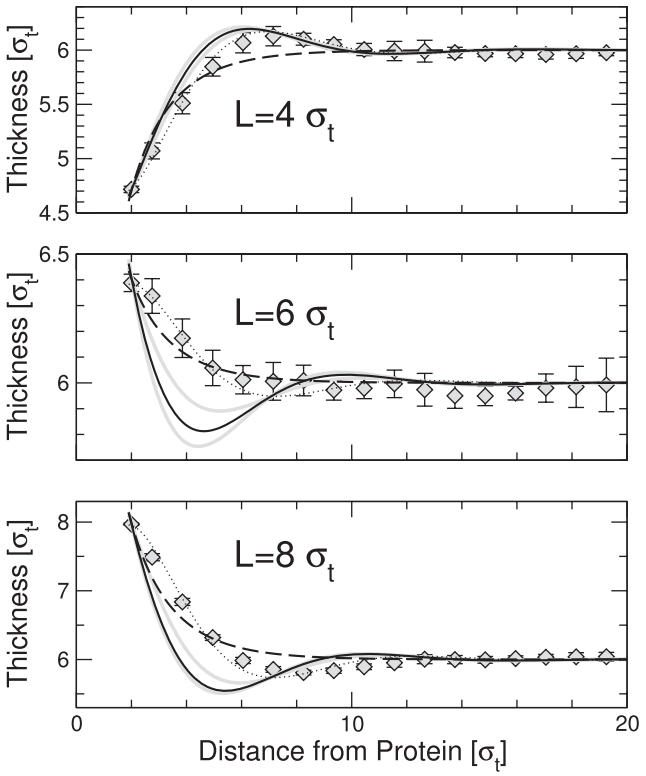

FIGURE 5 Membrane thickness profiles in the vicinity of an inclusion with hydrophobic thickness $L = 4\sigma_t$, $6\sigma_t$, and $8\sigma_t$, and hydrophobicity parameter $\epsilon_{pt} = 6$, compared with fits to the Landau-de Gennes theory (*dashed lines*), to the elastic theory with fixed $c_0 = -0.05/\sigma_t$ and $k_G = -0.26\epsilon$ (*solid lines*), and to the elastic theory with the additional fit parameter $\tilde{c}_0$ replacing c_0 (*dotted line*). The shaded lines indicate the range of the fit at fixed c_0 if c_0 and k_G are varied within the error given in Table 1.

monolayer. Two parameters are varied, the hydrophobicity parameter ϵ_{pt} (compare to Eq. 6) and the hydrophobic thickness L of the inclusion. The results for $\epsilon_{pt} = 2$ and 6 are shown in Fig. 4 for proteins with freely fluctuating orientations and for proteins with orientation constrained to the z axis. The deformation profiles induced by proteins with fixed and free orientations are identical within the error. This is due to the fact that proteins with free orientations were hardly tilted—the tilt angles were always smaller than ≤ 0.08. In the following, we shall only show data for proteins with fixed orientation.

Looking at Fig. 4, we first observe that the membrane thickness profiles are not strictly monotonic, but exhibit a characteristic over- or undershoot at the distance $r \sim 6\sigma_t$ from the protein. Such a weakly oscillatory behavior has also been observed in previous coarse-grained (61) and atomistic (80) simulations of protein-induced membrane deformations. In our case, the wavelength of the oscillation is roughly $\sim 10\sigma_t$, hence it can be related to the soft peristaltic mode in the fluctuation spectrum.

The second observation is that the protein hydrophobicity parameter ϵ_{pt} must exceed a certain value to produce classical hydrophobic mismatch. If ϵ_{pt} is too small, the protein effectively repels the lipids, and the membrane thickness is reduced at the surface of the protein regardless of the value of L. The hydrophobic section of the protein pins the membrane thickness for hydrophobicity parameters larger than $\epsilon_{pt} \sim 4$. This can be rationalized by noting that $\epsilon_{pt} \sim 4$ is the critical value where touching the protein surface is approximately as favorable for tail beads, from an energetic point of view, as being immersed in the bulk: The maximal contact energy of a tail bead in contact with a plane of tail beads is 4ϵ.

We proceed by fitting the profiles to the prediction of the analytical theories. Since the hydrophobicity of the inclusion must be larger than $\epsilon_{pt} > 4$ to cleave the membrane, we focus on the data for $\epsilon_{pt} = 6$. Fig. 5 compares them with fits to the prediction of the Landau-de Gennes theory (Eq. 10 and the elastic theory (Eq. 20 with the boundary conditions Eq. 18). In the Landau-de Gennes case, the three curves were fitted simultaneously with one common fit parameter ξ and three separate fit parameters $t_R = t_R^{\mathrm{LdG}}$. Not surprisingly,

TABLE 2 Parameters t_R^{LdG} and t_R^{el} (monolayer deformation at the surface of the inclusion) and $\tilde{c}_0$ (renormalized curvature) obtained from fitting the deformation profiles for large hydrophobicity parameters $\epsilon_{pt} = 5$ and 6 to the Landau-de Gennes theory (t_R^{LdG}) and to the elastic theory (t_R^{el} and $\tilde{c}_0$)

L [σ_t]	t_R^{LdG} [σ_t]	t_R^{el} [σ_t]	$\tilde{c}_0$ [σ_t^{-1}]
4	−0.94 ± 0.02	−0.66 ± 0.02	−0.11 [−0.12 − −0.10]
6	0.3 ± 0.02	0.18 ± 0.02	0.05 [− 0.03 − 0.06]
8	1.44 ± 0.02	0.93 ± 0.01	0.22 [0.15 − 0.26]

The remaining fit parameter in the Landau-de Gennes fit is the decay length $\xi = 2.0 \pm 0.1\sigma_t$. The uncertainty of $\tilde{c}_0$ results from the uncertainty of k_G.

the Landau-de Gennes fit cannot reproduce the oscillatory component of the profiles; otherwise, the fit is quite reasonable (Fig. 5, *dashed line*).

The thick solid lines in Fig. 5 show the fits to the elastic theory with $t_R = t_R^{el}$ as sole fit parameter. None of them is satisfactory. Hence the pure version of the elastic theory, which explains the profiles in terms of bulk membrane properties only, is not sufficient. In contrast, the data can be fitted very nicely if we release the constraint on the value of c_0, i.e., replace the spontaneous curvature by a renormalized curvature $\tilde{c}_0$ (*thin dotted lines* in Fig. 5, *solid lines* in Fig. 4). The resulting fit parameter values are essentially the same for $\epsilon_{pt} = 6$ (Fig. 5) and $\epsilon_{pt} = 5$ (data not shown) and given in Table 2.

From the fit results for t_R, we can infer the effective hydrophobic thickness $L_{eff} = 2(t_0 + t_R)$ of the inclusions. We note that the exact relation between t_R and the model parameter L is not a priori clear, since the lipid-protein potential is smooth and varies on the length scale σ_t. In all cases, the values for L_{eff} are reasonably close to L, i.e., well within $1\sigma_t$. The fit parameters for $\tilde{c}_0$, however, deviate considerably from the spontaneous curvature $c_0 = -0.05 \pm 0.02\sigma_t^{-1}$ (see Table 1) and depend on L. This clearly demonstrates that the local structure of the lipids that surround the inclusion indeed contributes to the boundary conditions, as has been discussed in Eq. 24.

A similar effect has been observed by Brannigan and Brown in a different coarse-grained model (32), and could be explained satisfactorily by the effect of nonconstant lipid volume. The volume per lipid in that model varies substantially over a range of r. In our model, the lipid volume (i.e., the lipid density inside the membrane) is almost constant throughout the system. Fig. 6 (*upper left*) shows profiles of the lipid bead density in the membrane for different hydrophobic thicknesses L at $\epsilon_{pt} = 6$. Here the lipid bead density ρ_l is defined as the number of lipid beads per area divided by the membrane thickness, and it is directly related to the local lipid volume v_l via $v_l = n/\rho_l$ with the chain length $n = 7$. Apart from an enhancement directly at the protein surface, which reflects the attractive protein-lipid interaction, and a very shallow depletion zone thereafter, the lipid density is nearly constant. Moreover, the curves for different hydrophobic thickness L are almost identical. Hence lipid volume effects contribute at most an L-independent constant to the renormalized curvature (24).

Fig. 6 also displays profiles of other candidate quantities that might affect the membrane properties and renormalize the curvature term at the surface. The upper-right panel shows the nematic order parameter for single bonds, $S_z = \langle 3(u_z/u)^2 - 1)\rangle/2$, where u refers to the bond vectors. The profiles show that the nematic order is enhanced in the vicinity of the inclusion. This is partly related to the increase of lipid density at the inclusion, since both quantities are correlated. The details of the nematic order profile, however, cannot be explained by the density profile alone. The ordering effect is highest for positively mismatched inclusions. Surprisingly, negatively mismatched inclusions induce higher order at the boundary than hydrophobically matching inclusions. This may seem counterintuitive at first, but becomes plausible in view of the fact that the monolayers also overlap in the vicinity of negatively mismatched inclusions. At larger distances from the inclusion, the bond order decays monotonically for hydrophobically matching and positively mismatched inclusions, and exhibits a nonmonotonic dip for negatively mismatched inclusions.

The middle panel in Fig. 6 shows two quantities that are related to the shielding of the hydrophobic membrane interior from the solvent. Since shielding is achieved by the heads, the areal head density gives a direct measure of the effectiveness of shielding. At constant lipid volume, however, the areal head density depends directly on the monolayer thickness $t(r)$ and thus does not qualify as independent field $\delta q(r)$ in the elastic theory, i.e., it cannot contribute directly to Eq. 24. Instead, we must consider a renormalized shielding parameter, such as, e.g., the hydrophilic shielding parameter introduced by de Meyer et al. (51). It is defined as the areal head density divided by the areal tail density, normalized such that it becomes one far from the inclusion. In the original version of the elastic theory, this parameter would be constant. Our data show that the areal head density is enhanced directly at the surface of the inclusion for all L—an indirect consequence of the attractive protein-tail interaction. The subsequent behavior depends on the type of mismatch: For positively mismatched inclusions, the areal head density goes up, for negatively mismatched inclusions, it goes down (Fig. 6, *middle left panel*). The hydrophilic shielding parameter (*middle right panel*) shows the same behavior at intermediate distances from the inclusion: Overshielding for positively mismatched inclusions, undershielding for negatively mismatched inclusions. Close to the inclusion, the curves turn around, in qualitative agreement with the observations of de Meyer et al. (51). The resulting integral $\int dr\ \delta q(r)/q_0$ (the K_2 term in Eq. 24) is roughly zero for $L = 6\sigma_t$ and $8\sigma_t$ and positive for $L = 4\sigma_t$.

The bottom panel in Fig. 6 shows profiles of the monolayer overlap, which measures the amount of interdigitation between monolayers. It has been calculated following two different conventions: The left graph shows a chain-related

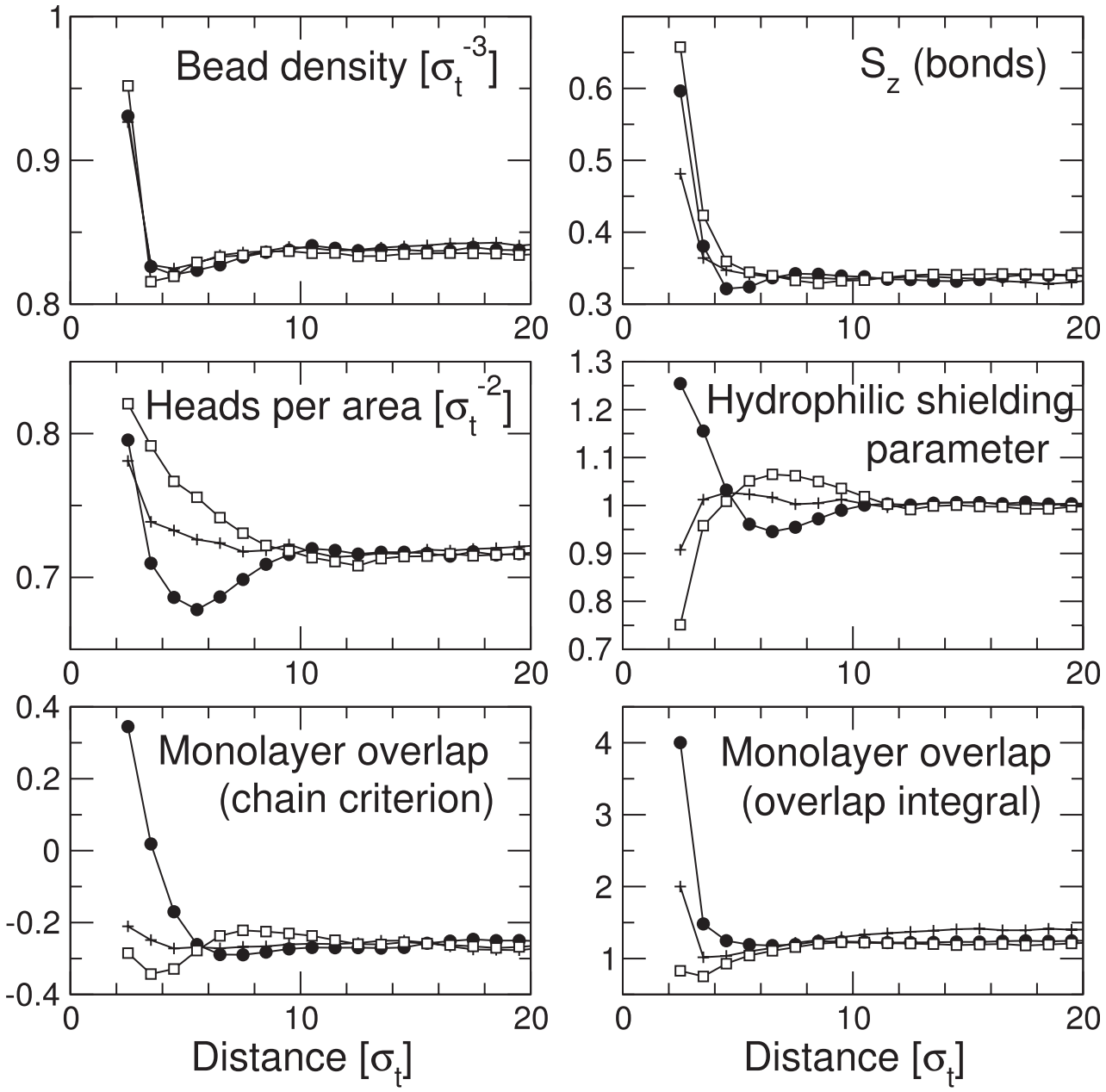

FIGURE 6 Radial profiles of various quantities as a function of the distance from the center of an inclusion with hydrophobic thickness $L = 4\sigma_t$ (*solid circles*), $L = 6\sigma_t$ (*crosses*), and $L = 8\sigma_t$ (*open squares*) at $\epsilon_{pt} = 6$. (*Upper left*) Bead density in the bilayer. (*Upper right*) Nematic order parameter for bonds. (*Middle left*) Heads per area in the monolayers. (*Middle right*) Hydrophilic shielding parameter (see text and (51)). (*Lower left* and *lower right*) Monolayer overlap, evaluated according to two different prescriptions (see text for definitions).

overlap parameter originally introduced by Kranenburg et al. (81): It is defined as $O_{\text{chain}} = \langle 2(l_z - t_0)/l_z \rangle$, where l_z is the z component of the end-to-end vector of chains and t_0 the monolayer thickness. Far from the inclusion, this parameter is negative, indicating that the two monolayers are well separated. Close to the inclusion, it becomes positive for negatively mismatched inclusions—the inclusions pull the lipids inwards and enforce a certain amount of interdigitation. For hydrophobically matching inclusions and for positively mismatched inclusions, it remains negative and roughly constant. The right graph shows a monomer-related overlap parameter which is defined as the overlap integral of the density profiles of the two monolayers, $O_{\text{bead}} = \int \mathrm{d}z \, (\rho_{\text{tail}}^{\text{upper}}(z) \times \rho_{\text{tail}}^{\text{lower}}(z))$, where ρ_{tail} denotes the density of tail beads. The curves for O_{bead} are qualitatively similar to those for O_{chain}, except that they are shifted to positive values—even far from inclusions, the monolayer densities have some overlap in the center of the bilayer (compare to Fig. 3).

To summarize this section, we find that the thickness deformation profiles around single inclusions can be fitted reasonably well with the exponential law predicted by the Landau-de Gennes theory. The fit with the pure version of the elastic theory is not good, but the elastic fit becomes much better and far superior to the Landau-de Gennes fit, if we allow for the possibility of curvature renormalization in the vicinity of the inclusion. We have identified a number of quantities which could conceivably contribute to this renormalization, i.e., they vary substantially close to the inclusion and they show a sizeable L-dependence. However, we cannot pinpoint an obvious single culprit. According to Table 2, the renormalized curvature $\tilde{c}_0$ exhibits an almost perfect linear dependence on the hydrophobic thickness L of the inclusion: The relation $\tilde{c}_0 - c_0 \approx 0.078/\sigma_t + 0.0825\,(L - 2t_0)/\sigma_t^2$ describes the data in Table 2 within 4%. None of the quantities shown in Fig. 6 produces such a linear behavior in an obvious way. We conclude that we have either still missed the truly relevant quantity, or that the observed linear relation is accidental and results from interplay of various curvature-renormalizing factors. From a physical point of view, it seems likely that most or all of the quantities discussed above will affect the local membrane properties, and most notably, the spontaneous curvature: Monolayer overlap will favor negative spontaneous curvature, since the area per tail increases. Variations in the hydrophilic shielding parameter will change the local pressure profile and hence affect the local curvature. Chain order will favor positive spontaneous curvature, since the structure in the chain region resembles that in the gel state, where the spontaneous curvature is large and positive.

Effective interactions between two proteins

Finally, we turn to studying the membrane-mediated interactions between inclusions. We study the dilute protein limit, i.e., we do not consider effects from multibody interactions between several proteins. To determine the potential of mean force, we have carried out simulations of membranes containing two inclusions and determined their radial pair distribution function. The effective potential $w(r)$ is

$$w(r) = -k_B T \ln g(r), \tag{33}$$

where k_B is the Boltzmann constant and T the temperature. Since the function $g(r)$ varies over several orders of magnitude, we have used umbrella sampling and reweighting to determine it accurately at all distances r.

The resulting potential curves are shown in Fig. 7 for several values of the hydrophobicity parameter ϵ_{pt} and the hydrophobic thickness L. The most striking feature of these profiles is their distinctly oscillatory shape. The oscillations have a wavelength of roughly $1\sigma_t$ in all systems, which indicates that they are caused by lipid packing in the vicinity of the inclusions. Only for the lowest value of the hydrophobicity parameter, $\epsilon_{pt} = 1$, the oscillatory structure disappears.

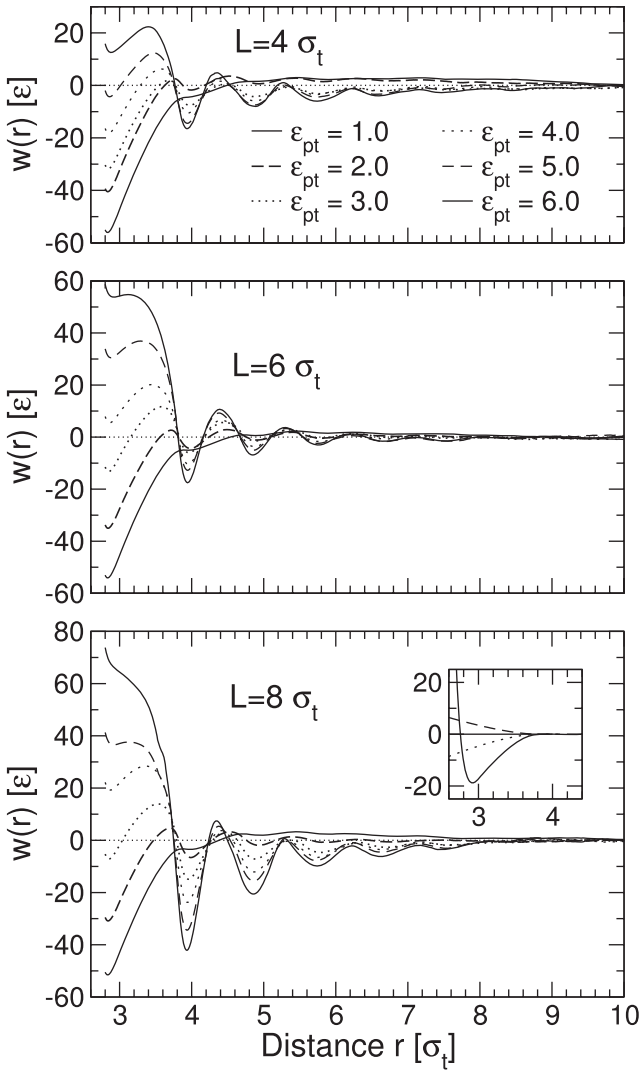

FIGURE 7 Potential of mean force between two inclusions with hydrophobic thickness $L = 4\sigma_t$ (negative mismatch, *top panel*), $L = 6\sigma_t$ (no mismatch, *middle panel*), and $L = 8\sigma_t$ (positive mismatch, *bottom panel*) for different values of the hydrophobicity parameter ϵ_{pt} as indicated. The inset in the bottom panel shows the interactions generated outside of the membrane (solvent-mediated depletion interaction and direct interaction) for hydrophobically matched inclusions (*solid line*), and the additional contribution of solvent-induced interactions at $L = 4\sigma_t$ (*dashed line*) and $L = 8\sigma_t$ (*dotted line*).

Here, we recover qualitatively the behavior observed in the simulations of purely repulsive inclusions by Sintes and Baumgärtner (52) and predicted by the corresponding molecular mean-field theories (37–39): The potential of mean force exhibits a minimum at close inclusion distances followed by a shallow maximum.

Beyond $r > 3.5\ \sigma_t$, all layering minima obey the general rule that they become more shallow with increasing protein separation r and/or decreasing hydrophobicity parameter ϵ_{pt}. The layering effects are most pronounced at high ϵ_{pt}, indicating that lipids pack more tightly if they move closer to the protein surface. In contrast, the first potential minimum at

$r \sim 3\ \sigma_t$ features the opposite behavior: It deepens as ϵ_{pt} decreases and disappears for high ϵ_{pt}. This minimum results from a number of effects that are not directly related to layering:

1. The direct protein-protein interaction and the solvent-induced depletion interaction between the hydrophilic protein section located outside of the membrane: This contribution is roughly constant and can be calculated analytically (*inset* of Fig. 7).
2. A depletion-type interaction induced by the lipids: By pushing the proteins toward each other, they maximize their translational and conformational entropy. This effect is strongest at low ϵ_{pt}, where the protein and the lipids effectively repel each other.
3. A bridging interaction induced by the lipids: At higher ϵ_{pt}, the lipids gain from being in contact with the proteins. Therefore, they tend to squeeze themselves between the proteins, pushing them apart, and the height of the first minimum goes up.

The competition between the depletion interaction and the lipid bridging effect accounts for the phenomenon reported earlier (Fig. 1), that the preferred arrangement of inclusions in the membrane depends on ϵ_{pt}: Weakly hydrophobic inclusions tend to touch each other, whereas strongly hydrophobic inclusions favor a larger distance where they are separated by one single lipid layer.

The influence of hydrophobic mismatch on the potential of mean force can be assessed by comparing the potential curves for different hydrophobic thickness L. On the one hand, hydrophobic mismatch affects the local features of the potential—the packing interaction (the strength of the layering) and the effective contact energy of proteins. On the other hand, it also contributes a smooth attractive interaction for mismatched proteins with $L = 4\sigma_t$ and $8\sigma_t$, which superimposes the oscillatory packing interaction at $r > 4\sigma_t$. It is worth noting that the sign of the additional term is independent of the type of mismatch—it is attractive for both positively and negatively mismatched inclusions. This smooth long-range contribution to the potential can now be compared with the predictions of the analytical theories.

Fig. 8 shows the corresponding curves for the Landau-de Gennes theory (*thin lines*) and the elastic theory (*thick lines*). They were calculated numerically by minimizing the free energy—Eq. 9 or Eq. 15 with $\tilde{c}_0$ replacing c_0—for systems containing two inclusions at given distance r, with the boundary condition $\phi = t_R$ at the surface of the inclusion. The model parameters were taken from Tables 1 and 2. In the Landau-de Gennes calculation, the parameter $4a$ in Eq. 9 was identified with the reduced area compressibility coefficient $k_A/{t_0}^2$ in Table 1. This may seem inconsistent, since the latter was originally determined from a fit of the fluctuation spectra to the elastic theory. Unfortunately, the fit of the spectra to the Landau-de Gennes theory (Fig. 2) did not produce dependable parameters a and c. The value of k_A in Table 1 is compatible with independent simulation data on the lipid-

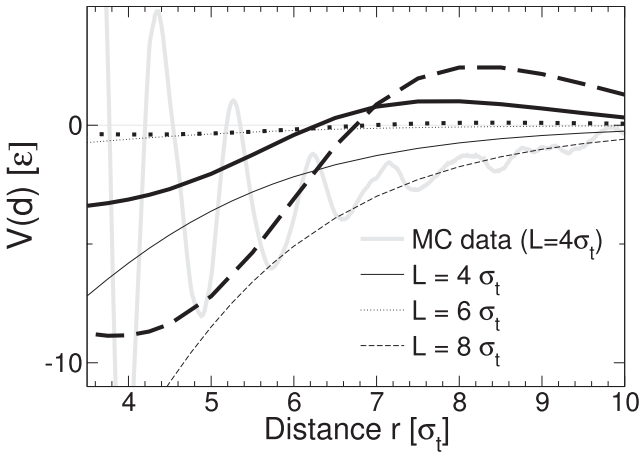

FIGURE 8 Effective interaction potential between two inclusions according to the Landau-de Gennes theory (*thin lines*) and the elastic theory (*thick lines*) for inclusions with different hydrophobic thickness L as indicated. The thick shaded line shows the simulation data for $L = 4\sigma_t$, $\epsilon_{pt} = 6$ for comparison.

area increase at finite surface tension (J. Neder, unpublished data) and was thus considered to be more reliable. The value for c then follows from $c = \xi^2 a$, using the value $\xi = 2.0\sigma_t$ determined from the fit to the membrane thickness profiles around single inclusions.

To calculate the free energy, we have discretized the corresponding integrals in real space using a square grid with spatial discretization parameter h and a second-order difference scheme to evaluate the derivatives. The boundary condition was implemented by setting $\phi = t_R$ inside the inclusion. (The other boundary condition of the elastic theory, Eq. 18, follows automatically from the energy minimization.) The energy was minimized via a steepest descent method, using a relaxation scheme introduced in Schmid and Schick (83). The final accuracy was $\int d^2r|\delta F/\delta\phi| \leq 10^{-6}$. The curves shown in Fig. 8 were obtained using the spatial discretization $h = 0.25\sigma_t$ and a system of size $30 \times 20{\sigma_t}^2$ with periodic boundary conditions, which corresponds to the situation in the Monte Carlo simulations. Calculations for $h = 0.5\sigma_t$ and system sizes up to $70 \times 50{\sigma_t}^2$ produced the same curves, hence discretization errors and finite size effects are negligible.

Both the Landau-de Gennes theory and the elastic theory predict an attractive interaction at distances $r < 6\sigma_t$, in agreement with the trend observed in the simulation data. For larger distances, the elastic theory predicts the potential of mean force to become positive and exhibit a peak at $r \sim 8\sigma_t$. The simulation data show no indication for the existence of such a positive peak. Apparently, the elastic theory fails to reproduce the trend of the simulation data at large distances, which is surprising, since this is where one would expect it to work best. The potential predicted by the Landau-de Gennes theory is negative and attractive everywhere and thus better compatible with the data. However, this should not be overrated, given the overall poorer performance of this approach

when looking at pure membranes and membrane interactions with single inclusions. The weakly oscillatory behavior of the potential of mean force in the elastic theory is generated by the soft peristaltic mode in the fluctuation spectrum, which has been shown to leave a clear signature in the shape of the distortion profiles around single proteins. The simulation data suggest that the effect of this mode on the lipid-mediated interactions between two proteins is destroyed by some yet unknown mechanism.

SUMMARY AND CONCLUSION

To summarize, we have determined protein-membrane interactions and calculated lipid-mediated interactions between proteins in a simple generic molecular model for lipid bilayers, and compared the results to the predictions of two popular continuum theories. Whereas the effect of the protein-membrane interactions on the deformation profiles (Fig. 4) can be described very nicely by a theory that essentially treats the membrane as a pair of coupled elastic sheets (monolayers), the local lipid structure clearly dominates the shape of the membrane-induced protein-protein interactions.

We note that the specific shape of these packing interactions depends sensitively on the microscopic details of the system. All liquids have a local liquid structure, and packing effects will clearly also be present in real membranes. However, their contribution to the potential of mean force will differ from that in our model. In particular, the amplitude of oscillations will presumably be much smaller, since packing effects are most likely overestimated in our simple Lennard-Jones bead model. Hence the potentials of mean force shown in Fig. 7 cannot be related to the potentials of mean force of proteins in membranes in real systems in a quantitative sense. At a qualitative level, however, some conclusions can be drawn.

We have identified several factors that may contribute to the effective potential between cylindrical proteins in our simple model membranes: 1), Direct protein-protein interactions; 2), depletion interactions; 3), lipid bridging interactions; 4), packing interactions; and 5), elastic interactions. The interplay and competition of these factors determine the final, most favorable arrangement of proteins in the bilayer. Their relative importance is determined by the hydrophobicity of the proteins and the hydrophobic mismatch. The most dramatic effect of hydrophobic mismatch in our system can be associated with its influence on the factors 2–4. Thus we do observe a hydrophobic mismatch interaction, but the dominant contribution to this interaction seems related to local reordering effects, and not to the elasticity of the monolayers. Intriguingly, the elastic theory does not even describe correctly the smooth long-range part of the interaction.

As a general trend, the interaction tends to be attractive, i.e., it is most favorable for proteins to cluster. This is trivially the case for purely oscillatory interactions, but it also seems to hold for the additional smooth contribution, regardless of the type of mismatch. The observation is consistent with the findings of de Meyer et al. (51)—the potentials of mean force presented in that article are also always attractive, except for proteins with very large diameters. Whereas protein clustering may sometimes be desirable, it also has negative effects—for example, it reduces the mobility of the proteins in the membrane, it makes them less accessible for other proteins, etc. Our results thus raise the question whether the effects reported here have to be counteracted by external, not membrane-related protein interactions, or whether it is possible to identify mechanisms that induce repulsive membrane-mediated interactions between proteins, and stabilize protein dispersions, e.g., in mixed multicomponent membranes.

We thank Grace Brannigan and Jörg Neder for very helpful discussions. The simulations were mostly carried out at the Paderborn center for parallel computing (PC2) and the John von Neumann Institute for Computing computer center in Jülich.

This work was funded by the German Science Foundation (DFG) within the SFB No. 613. F.L.H.B. is partially supported by the National Science Foundation (grant No. CHE-0349196). F.L.H.B. is a Sloan Research Fellow and a Camille Dreyfus Teacher-Scholar.

REFERENCES

1. Gennis, R. B. 1989. Biomembranes—Molecular Structure and Function. Springer Verlag, New York.
2. Rasband, M. N., and J. S. Trimmer. 2001. Developmental clustering of ion channels at and near the node of Ranvier. *Dev. Biol.* 236:5–16.
3. Elliott, J., D. Needham, J. Dilger, and D. Haydon. 1983. The effects of bilayer thickness and tension on gramicidin single-channel lifetimes. *Biochim. Biophys. Acta.* 735:95–103.
4. Botelho, A. V., T. Huber, T. P. Sakmar, and M. F. Brown. 2006. Curvature and hydrophobic forces drive oligomerization and modulate activity of rhodopsin in membranes. *Biophys. J.* 91:4464–4477.
5. Mouritsen, O. G., and M. Bloom. 1993. Models of lipid-protein interactions in membranes. *Annu. Rev. Biophys. Biomol. Struct.* 22:145–171.
6. Gil, T., J. H. Ipsen, O. G. Mouritsen, M. C. Sabra, M. M. Sperotto, et al. 1998. Theoretical analysis of protein organization in lipid membranes. *Biochim. Biophys. Acta. Rev. Biomembr.* 1376:245–266.
7. Sperotto, M. M., S. May, and A. Baumgärtner. 2006. Modeling of proteins in membranes. *Chem. Phys. Lipids.* 141:2–29.
8. Edidin, M. 2003. The state of lipid rafts: from model membranes to cells. *Annu. Rev. Biophys. Biomol. Struct.* 32:257–283.
9. Bloom, M., E. Evans, and O. G. Mouritsen. 1991. Physical properties of the fluid lipid-bilayer component of cell membranes: a perspective. *Q. Rev. Biophys.* 24:293–397.
10. Killian, J. A. 1998. Hydrophobic mismatch between proteins and lipids in membranes. *Biochim. Biophys. Acta Rev. Biomembr.* 1376:401–416.
11. Dumas, F., M. C. Lebrun, and J. F. Tocanne. 1999. Is the protein/lipid hydrophobic matching principle relevant to membrane organization and functions? FEBS Lett. 458:271–277.
12. Harroun, T. A., W. T. Heller, T. M. Weiss, L. Yang, and H. W. Huang. 1999. Experimental evidence for hydrophobic matching and membrane-mediated interactions in lipid bilayers containing gramicidin. *Biophys. J.* 76:937–945.
13. Sharpe, S., K. R. Barber, C. W. M. Grant, D. Goodyear, and M. R. Marrow. 2002. Organization of model helical peptides in lipid bilayers:

insight into the behavior of single-span protein transmembrane domains. *Biophys. J.* 83:345–358.

14. De Planque, M. R. R., and J. A. Killian. 2003. Protein-lipid interactions studied with designed transmembrane peptides: role of hydrophobic matching and interfacial anchoring. *Review. Mol. Membr. Biol.* 20:271–284.
15. Owicki, J. C., M. W. Springgate, and H. M. McConnell. 1978. Theoretical study of protein-lipid interactions in bilayer membranes. *Proc. Natl. Acad. Sci. USA.* 75:1616–1619.
16. Owicki, J. C., and H. M. McConnell. 1979. Theory of protein-lipid and protein-protein interactions in bilayer membranes. *Proc. Natl. Acad. Sci. USA.* 76:4750–4754.
17. Jensen, M. O., and O. G. Mouritsen. 2004. Lipids do influence protein function—the hydrophobic matching hypothesis revisited. *Biochim. Biophys. Acta.* 1666:205–226.
18. Mouritsen, O. G., and M. Bloom. 1984. Mattress model of lipid-protein interactions in membranes. *Biophys. J.* 36:141–153.
19. Fattal, D. R., and A. Ben-Shaul. 1993. A molecular model for lipid-protein interaction in membranes: the role of hydrophobic mismatch. *Biophys. J.* 65:1795–1809.
20. Fattal, D. R., and A. Ben-Shaul. 1995. Lipid chain packing and lipid-protein interaction in membranes. *Physica A.* 220:192–216.
21. Kralchevski, P. A., V. N. Paunov, N. D. Denkov, and K. Nagayama. 1995. Stresses in lipid membranes and interactions between inclusions. *Faraday Trans.* 91:3415–3432.
22. Bohinc, K., V. Kralj-Iglic, and S. May. 2003. Interaction between two cylindrical inclusions in a symmetric lipid bilayer. *J. Chem. Phys.* 119:7435–7444.
23. Huang, H. W. 1986. Deformation free energy of bilayer membrane and its effect on gramicidin channel lifetime. *Biophys. J.* 50:1061–1070.
24. Huang, H. W. 1995. Elasticity of lipid bilayer interacting with amphiphilic helical peptides. *J. Physique II Fr.* 5:1427–1431.
25. Harroun, T. A., W. T. Heller, T. M. Weiss, L. Yang, and H. W. Huang. 1999. Theoretical analysis of hydrophobic matching and membrane-mediated interactions in lipid bilayers containing gramicidin. *Biophys. J.* 76:3176–3185.
26. Nielsen, C., M. Goulian, and O. S. Andersen. 2000. Energetics of inclusion-induced bilayer deformations. *Biophys. J.* 74:1966–1983.
27. Nielsen, C., and O. S. Andersen. 2000. Inclusion-induced bilayer deformations: effects of monolayer equilibrium curvature. *Biophys. J.* 79:2583–2604.
28. Dan, N., P. Pincus, and S. A. Safran. 1993. Membrane induced interactions between inclusions. *Langmuir.* 9:2768–2771.
29. Dan, N., A. Berman, P. Pincus, and S. A. Safran. 1994. Membrane induced interactions between inclusions. *Journal de Physique II.Fr.* 4:1713–1725.
30. Aranda-Espinoza, H., A. Berman, N. Dan, P. Pincus, and S. Safran. 1996. Interaction between inclusions embedded in membranes. *Biophys. J.* 71:648–656.
31. Brannigan, G., and F. L. H. Brown. 2006. A consistent model for thermal fluctuations and protein-induced deformations in lipid bilayer. *Biophys. J.* 90:1501–1520.
32. Brannigan, G., and F. L. H. Brown. 2007. Contributions of Gaussian curvature and nonconstant lipid volume to protein deformations of lipid bilayers. *Biophys. J.* 92:864–876.
33. van Duyl, B. Y., D. T. S. Rijkers, B. De Kruijff, and J. A. Killian. 2002. Influence of hydrophobic mismatch and palmitoylation on the association of transmembrane α-helical peptides with detergent-resistant membranes. *FEBS Lett.* 523:79–84.
34. De Planque, M. R. R., B. B. Bonev, J. A. A. Demmers, D. V. Greathouse, R. E. Koeppe, et al. 2003. Interfacial anchor properties of tryptophan residues in transmembrane peptides dominate over hydrophobic matching effects in peptide-lipid interactions. *Biochemistry.* 42:5341–5348.
35. Ben-Shaul, A., N. Ben-Tal, and B. Honig. 1996. Statistical thermodynamic analysis of peptide and protein insertion into lipid membranes. *Biophys. J.* 71:130–137.
36. Lagüe, P., M. J. Zuckermann, and B. Roux. 1998. Protein inclusion in lipid membranes: a theory based on the hypernetted chain integral equation. *Faraday Discuss.* 111:165–172.
37. Lagüe, P., M. J. Zuckermann, and B. Roux. 2000. Lipid-mediated interactions between intrinsic membrane proteins: a theoretical study based on integral equations. *Biophys. J.* 79:2867–2879.
38. Lagüe, P., M. J. Zuckermann, and B. Roux. 2001. Lipid-mediated interactions between intrinsic membrane proteins: dependence on protein size and lipid composition. *Biophys. J.* 81:276–284.
39. May, S., and A. Ben-Shaul. 2000. A molecular model for lipid-mediated interaction between proteins in membranes. *Phys. Chem. Chem. Phys.* 2:4494–4502.
40. Natali, F., A. Relini, A. Gliozzi, R. Rolandi, P. Cavatorta, et al. 2003. Protein-membrane interaction: effect of myelin basic protein on the dynamics of oriented lipids. *Chem. Phys.* 292:455–464.
41. Kota, Z., T. Pali, and D. Marsh. 2004. Orientation and lipid-peptide interactions of gramicidin a in lipid membranes: polarized attenuated total reflection infrared spectroscopy and spin-label electron spin resonance. *Biophys. J.* 86:1521–1531.
42. May, S. 2000. Theories on structural perturbations of lipid bilayers. *Curr. Opin. Colloid Interface Sci.* 5:244–249.
43. Goulian, M., R. Bruinsma, and P. Pincus. 1993. Long-range forces in heterogeneous fluid membranes. *Europhys. Lett.* 22:145–150.
44. Netz, R. R., and P. Pincus. 1995. Inhomogeneous fluid membranes—segregation, ordering and effective rigidity. *Phys. Rev. E Stat. Phys. Plasmas Fluids Relat. Interdiscip. Topics.* 52:4114–4128.
45. Golestanian, R., M. Goulian, and M. Kardar. 1996. Fluctuation-induced interactions between rods on membranes and interfaces. *Europhys. Lett.* 33:241–245.
46. Weikl, T. R. 2001. Fluctuation-induced aggregation of rigid membrane inclusions. *Europhys. Lett.* 54:547.
47. Reynwar, B. J., G. Illya, V. A. Harmandaris, M. M. Müller, K. Kremer, et al. 2007. Aggregation and vesiculation of membrane proteins by curvature-mediated interactions. *Nature.* 447:461–464.
48. Fournier, J. -B. 1999. Microscopic membrane elasticity and interactions among membrane inclusions: interplay between the shape, dilation, tilt and tilt-difference modes. *Eur. Phys. J. B.* 11:261–272.
49. Lenz, O., and F. Schmid. 2007. Structure of symmetric and asymmetric ripple phases in lipid bilayers. *Phys. Rev. Lett.* 98:058104.
50. Efremov, R. G., D. E. Nolde, A. G. Konshina, N. P. Syrtcev, and A. S. Arseniev. 2004. Peptides and proteins in membranes: what can we learn via computer simulations? Curr. Med. Chem. 11:2421–2442.
51. de Meyer, F., M. Venturoli, and B. Smit. 2008. Molecular simulations of lipid mediated protein-protein interactions. *Biophys. J.* 95:1851–1865.
52. Sintes, T., and A. Baumgärtner. 1997. Protein attraction in membranes induced by lipid fluctuations. *Biophys. J.* 73:2251–2259.
53. Smeijers, A. F., K. Pieterse, A. J. Markvoort, and P. A. J. Hilbers. 2006. Coarse-grained transmembrane proteins: hydrophobic matching, aggregation, and their effect on fusion. *J. Phys. Chem. B.* 110:13614–13623.
54. Marrink, S. J., H. J. Risselada, S. Yefimov, D. P. Tielemann, and A. H. de Vries. 2007. The MARTINI force field: coarse-grained model for biomolecular simulations. *J. Phys. Chem. B.* 111:7812–7823.
55. Schmid, F., D. Düchs, O. Lenz, and B. West. 2007. A generic model for lipid monolayers, bilayers, and membranes. *Comput. Phys. Commun.* 177:168–171.
56. Stadler, C., H. Lange, and F. Schmid. 1999. Short grafted chains: Monte Carlo simulations of a model for monolayers of amphiphiles. *Phys. Rev. E Stat. Phys. Plasmas Fluids Relat. Interdiscip. Topics.* 59:4248–4257.
57. Düchs, D., and F. Schmid. 2001. Phase behavior of amphiphilic monolayers: theory and simulations. *J. Phys. Condens. Matter.* 13:4853–4862.
58. Lenz, O., and F. Schmid. 2005. A simple computer model for liquid lipid bilayers. *J. Mol. Liq.* 117:147–152.

59. Lenz, O. 2007. Computer simulations of lipid bilayers. Dissertation, Universität Bielefeld, Germany.

60. Sperotto, M. M., and O. G. Mouritsen. 1991. Monte Carlo simulation of lipid order parameter profiles near integral membrane proteins. *Biophys. J.* 59:261–270.

61. Venturoli, M., B. Smit, and M. M. Sperotto. 2005. Simulation studies of protein-induced bilayer deformations, and lipid-induced protein tilting, on a mesoscopic model for lipid bilayers with embedded proteins. *Biophys. J.* 88:1778–1798.

62. Venturoli, M. 2004. Mesoscopic models of lipid bilayers and bilayers with embedded proteins. PhD thesis, University of Amsterdam, The Netherlands.

63. Helfrich, P., and E. Jakobsson. 1990. Calculation of deformation energies and conformations in lipid membranes containing gramicidin channels. *Biophys. J.* 57:1075–1084.

64. Reference deleted in proof.

65. Reference deleted in proof.

66. Fournier, J. -B. 1998. Coupling between membrane tilt-difference and dilation: a new ''ripple'' instability and multiple crystalline inclusions phases. *Europhys. Lett.* 43:725–730.

67. Fošnariè, M., A. Igliè, and S. May. 2006. Influence of rigid inclusions on the bending elasticity of a lipid membrane. *Phys. Rev. E Stat. Nonlin. Soft Matter Phys.* 74:051503.

68. Harries, D., and A. Ben-Shaul. 1997. Conformational chain statistics in a model lipid bilayer: comparison between mean field and Monte Carlo calculations. *J. Chem. Phys.* 106:1609–1619.

69. Goetz, R., G. Gompper, and R. Lipowsky. 1999. Mobility and elasticity of self-assembled membranes. *Phys. Rev. Lett.* 82:221–224.

70. Lindahl, E., and O. Edholm. 2000. Mesoscopic undulations and thickness fluctuations in lipid bilayers from molecular dynamics simulations. *Biophys. J.* 79:426–433.

71. Marrink, S. J., and A. E. Mark. 2001. Effect of undulations on surface tension in simulated bilayers. *J. Phys. Chem. B.* 105:6122–6127.

72. Loison, C., M. Mareschal, K. Kremer, and F. Schmid. 2003. Thermal fluctuations in a lamellar phase of a binary amphiphile-solvent mixture: a molecular-dynamics study. *J. Chem. Phys.* 119:13138–13148.

73. Safran, S. A. 1994. Statistical Thermodynamics of Surfaces, Interfaces, and Membranes. Perseus Books, Cambridge, MA.

74. Irving, J. H., and J. G. Kirkwood. 1950. The statistical mechanical theory of transport processes. IV. The equations of hydrodynamics. *J. Chem. Phys.* 18:817–829.

75. Goetz, R., and R. Lipowsky. 1998. Computer simulations of bilayer membranes: self-assembly and interfacial tension. *J. Chem. Phys.* 108:7397–7409.

76. Lindahl, E., and O. Edholm. 2000b. Spatial and energetic-entropic decomposition of surface tension in lipid bilayers from molecular dynamics simulations. *J. Chem. Phys.* 113:3882–3893.

77. Reference deleted in proof.

78. Reference deleted in proof.

79. Marsh, D. 2006. Elastic curvature constants of lipid monolayers and bilayers. *Chem. Phys. Lipids.* 144:146–159.

80. Cordomi, A., and J. J. Perez. 2007. Molecular dynamics simulations of rhodopsin in different one-component lipid bilayers. *J. Phys. Chem. B.* 111:7052–7063.

81. Kranenburg, M., M. Venturoli, and B. Smit. 2003. Phase behavior and induced interdigitation in bilayers studied with dissipative particle dynamics. *J. Phys. Chem. B.* 107:11491–11501.

82. Reference deleted in proof.

83. Schmid, F., and M. Schick. 1995. Liquid phases of Langmuir monolayers. *J. Chem. Phys.* 102:2080–2091.